Emergence of Classical Magnetic Order from Anderson Towers: Quantum Darwinism in Action

O. M. Sotnikov,[1,2] E. A. Stepanov,[3] M. I. Katsnelson,[4] F. Mila,[5] and V. V. Mazurenko[1,2,*]

[1]*Theoretical Physics and Applied Mathematics Department, Ural Federal University, Mira Street 19, 620002 Ekaterinburg, Russia*

[2]*Russian Quantum Center, Skolkovo, Moscow 121205, Russia*

[3]*CPHT, CNRS, École polytechnique, Institut Polytechnique de Paris, 91120 Palaiseau, France*

[4]*Radboud University, Institute for Molecules and Materials, Heyendaalseweg 135, 6525AJ Nijmegen, Netherlands*

[5]*Institute of Physics, École Polytechnique Fédérale de Lausanne (EPFL), CH-1015 Lausanne, Switzerland*

(Received 23 December 2022; revised 13 July 2023; accepted 11 October 2023; published 8 November 2023)

Environment is assumed to play a negative role in quantum mechanics, destroying the coherence in a quantum system and, thus, randomly changing its state. However, for a quantum system that is initially in a degenerate ground state, the situation could be different. In this case, the infinite manifold of ground state eigenfunctions can contain a few states of zero entanglement, which can be demonstrated based on the minimization of the von Neumann entropy. Then, following quantum Darwinism, these "classical" combinations are selected and promoted by the quantum environment, which means that different independent observers find them in experiments. In this work, we find and explore such classical states in the eigenspectra of skyrmionic and antiferromagnetic quantum systems starting from a numerical realization of Anderson's tower of states. The degeneracy of the quantum ground state is shown to be the key for explaining nontrivial properties of magnetic matter in the classical world including topological protection arising in the classical limit.

DOI: 10.1103/PhysRevX.13.041027

Subject Areas: Condensed Matter Physics, Magnetism, Quantum Physics

I. INTRODUCTION

Despite the huge success of quantum physics, which is one of the pillars of our science and technology, its foundations still remain the subject of hot debates, and many conceptual issues still require further investigations [1–7]. In particular, searching for the connection between quantum and classical descriptions of the same phenomenon or object has a long history in physics starting from the foundation of quantum mechanics. In this sense, the development of the path integral concept [8–10] is a bright example showing that the classical trajectory of a particle is just one of numerous alternatives characterized by different probabilities. In these terms, classicality means nothing but destruction of an interference between different alternatives, similar to the transition from wave to geometric optics [11].

*Corresponding author: vmazurenko2011@gmail.com

However, in the case of the classical-quantum correspondence, the problem is more complicated. The transition between the classical and quantum regimes cannot be determined only by the fact that the characteristic size of the system, which can be related to the de Broglie wavelength, becomes small compared to other length scales of the problem. According to the popular decoherence program, the classical-quantum correspondence is rather related to the openness of the quantum system and to the destruction of quantum interferences by the interaction with the environment [12–17]. The problem is closely related to the measurement problem [18]. According to Bohr's complementarity principle [19], a quantum measurement is nothing but the result of the interaction of a quantum particle with a classical measuring device. This picture is the basis of the formal theory of measurements developed by von Neumann [20]. This theory includes a mysterious collapse of the quantum wave function after the measurement. Further developments have led to a more complicated picture, including soft measurements [21] and decoherence waves in distributed quantum systems [22–24]. There are also analytical [25] and numerical [26] attempts to derive von Neumann's postulate from a consequent quantum consideration of the measurement process, including decoherence

by the environment. In general, the problem does not seem to be completely solved, and further attempts at clarifying these key issues are required.

These questions may look too general and too abstract, but, actually, they are closely related to a very common and important phenomenon of physics around us. Antiferromagnetism, a usual property of condensed matter [27], is, probably, one of the best examples. The classical Néel picture of magnetic sublattices for the case of an "antiferromagnetic" exchange interaction is in an obvious contradiction with quantum mechanics' prediction of a singlet ground state [27]. Actually, the antiferromagnetic state can be described without introducing sublattices [28], but its difference with the singlet state remains dramatic. A general way to establish the correspondence between quantum and classical descriptions of antiferromagnets was proposed in the seminal work of Anderson [29]. It has been shown there that in some cases linear combinations of eigenstates of a quantum Hamiltonian that form a tower of low-energy states can be related to an ordered state that would be the classical ground state of the system in the thermodynamic limit. Such a tower-of-states (TOS) approach may be of crucial importance, because it treats the fundamental problem of quantum-classical correspondence from a completely different perspective, namely, without referring to measurements or postulating decoherence due to the environment. Moreover, it has proven to be extremely helpful in detecting broken symmetries with an eigenspectrum of even small-size supercells of quantum systems. Up to now, the Anderson towers approach was mainly used for studying quantum antiferromagnets [30–32]. However, it is worth mentioning that the previous studies based on the group-theoretical calculations were fully concentrated on the symmetry identification of the eigenfunctions contributing to the TOS without attempting to quantify their partial contributions. Such an approach is also not flexible, since it requires one to know the exact symmetry of the reconstructed classical order, which prevents using the approach in the case where the system is characterized by a transition to an unknown classical state (a problem known as hidden order).

In this paper, we report on a symmetry-free numerical technique based on gradient-descent optimization for constructing TOS on the basis of a limited number of calculated low-lying eigenstates of a quantum system. In contrast to previous works, our approach provides quantitative information on the TOS composition. By means of the developed scheme, we explore representative antiferromagnetic systems and less trivial topologically protected classical magnetic skyrmions [33] that attract considerable attention due to their fundamental interest [34–36] and technological importance [37,38]. Recent theoretical studies [39–45] suggest that the ground state of some quantum spin Hamiltonians with competing isotropic and anisotropic interactions can be considered as analogs of classical skyrmions, since the magnetization, the susceptibility, and the scalar chirality calculated for these quantum ground states agree with those obtained for the corresponding classical models. For this reason, one can formally define the quantum skyrmion as a quantum state for which the spin-spin correlation functions reproduce the same quantities in the classical version of the problem. The natural question similar to the antiferromagnetic case is, then, what is the mechanism through which one can observe a classical skyrmion in a system that is *a priori* quantum?

In this work, we show that the connection between the classical and quantum systems can be established not only at the level of the observables, as done up to now, but also at the most general level of a quantum state and of macroscopic classical order *per se*. To this aim, we use the concept of Anderson's tower of states and explore both the towers of quantum wave functions to reconstruct classical solutions and the towers of classical configurations needed to reproduce the quantum ground state (see Fig. 1). The analysis of the composition of the TOS that we obtain for magnetic skyrmions and for antiferromagnets uncovers important details of Anderson's theory that are not addressed in previous group-theoretical considerations. We argue that the environment plays a crucial role in selecting specific combinations of the quantum states that build the TOS that correspond to classical order and are known as pointer states in decoherence theory (quantum Darwinism). Thus, quantum decoherence should be considered as an important part of the TOS theory. Since the

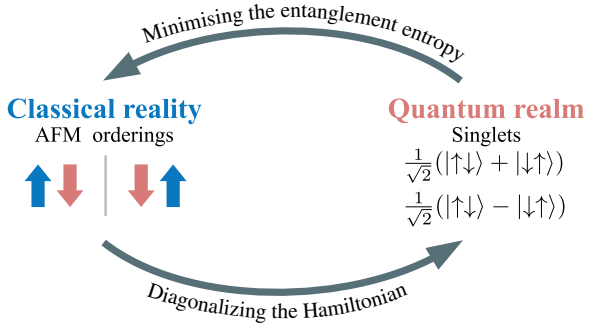

FIG. 1. Cartoon explaining the main idea of the paper, namely, how to go from classical ordered states to quantum low-lying states and vice versa without any explicit reference to the environment, on the example of the antiferromagnet. How to go from the coherent (classical) antiferromagnetic states to the low-lying exact eigenfunctions is "easy," because one just has to diagonalize the Hamiltonian in the basis of the coherent states. By contrast, to go from the low-lying quantum states to classical states is "difficult" in the sense that, according to the standard theory, it requires the interaction of the system with its environment. In this paper, we show that to go from the low-lying exact eigenstates to the classical states is also possible without any reference to the environment by minimizing in the Hilbert space of low-lying eigenstates the von Neumann entanglement entropy when cutting the system into two parts.

TOS analysis itself can be used as a more effective search for pointer states within the decoherence program, both theories benefit from this integration.

II. RESULTS

A. Protocol for constructing the Anderson tower

Formally, a quantum wave function corresponding to any classical spin texture can be defined as a product of coherent states of individual spins [46–48]:

$$|\Psi_T\rangle = \prod_i \left[\cos\frac{\theta_i}{2} e^{i(\phi_i/2)}|\uparrow\rangle + \sin\frac{\theta_i}{2} e^{-i(\phi_i/2)}|\downarrow\rangle\right], \quad (1)$$

where the polar angles θ_i and ϕ_i set a local basis for each spin. Below, we refer to this state as a coherent state or a target wave function. The consequent projective measurements [20] of the state Ψ_T in σ^z, σ^x, and σ^y bases result in a set of projections $\langle\hat{S}_i^z\rangle$, $\langle\hat{S}_i^x\rangle$, and $\langle\hat{S}_i^y\rangle$ for each spin. The latter can be associated with the direction of the classical magnetic moment $\mathbf{m}_i$ in magnetic structures measured in spin-polarized scanning tunneling microscopy experiments [49]. More specifically, $\langle m_i^x\rangle = \sin\theta_i\cos\phi_i$, $\langle m_i^y\rangle = \sin\theta_i\sin\phi_i$, and $\langle m_i^z\rangle = \cos\theta_i$. Thus, one can establish a formal connection between parameters of the coherent state and the classical magnetic moments of a quantum system observed in real or numerical experiments: $\theta_i = \arccos\langle m_i^z\rangle$ and $\phi_i = \arctan(\langle m_i^y\rangle/\langle m_i^x\rangle)$.

In order to construct the Anderson tower for a quantum system, we follow the key steps visualized in Figs. 2(a)–2(c). First, we perform the exact diagonalization of a quantum Hamiltonian and determine its eigenstates Ψ_n [Fig. 2(a)]. We consider only the low-lying part of the eigenspectrum $n \in [0, k]$ and introduce the initial approximation for the target wave function Ψ_A with random complex coefficients α_n [Fig. 2(b)]. Furthermore, these coefficients are varied using the gradient-descent method to get the maximal fidelity between Ψ_A and Ψ_T [Fig. 2(c)]. Here, as for any optimization procedure, the choice of the loss function that is responsible for the quality of the resulting approximation and convergence speed plays a central role. In this work, it is given by the following expression:

$$\mathbb{E}(\boldsymbol{\alpha}) = 1 - |\langle\Psi_T|\Psi_A(\boldsymbol{\alpha})\rangle|. \quad (2)$$

The coefficients are updated as

$$\boldsymbol{\alpha}_{\text{new}} = \boldsymbol{\alpha}_{\text{old}} - \gamma\frac{\partial\mathbb{E}}{\partial\boldsymbol{\alpha}_{\text{old}}}, \quad (3)$$

where γ is the gradient-descent step that is taken to be 1. This choice for the loss function can be justified by the fact that the fidelity is a standard metric to define the distance between two quantum states [50]. Within our approach, the loss function (2) can be replaced by another form with milder conditions, which might be useful in the case where the precise form of the target state Ψ_T is unknown.

An important property of the proposed numerical scheme for constructing TOS is that we can quantitatively control the quality of the approximation for Ψ_A with the parameter k that truncates the eigenspectrum. It is worth noting that in previous works the construction of the Anderson TOS for antiferromagnets is mainly based on a symmetry-based selection of the low-lying states of the eigenspectrum in order to find a signature of a symmetry-broken state that can be the ground state of the system in the thermodynamic limit [30–32,51]. However, a combination of these eigenstates taken with some amplitudes into a concrete coherent wave function and exploring its properties by calculating different observables are beyond the capabilities of the group-theoretical approach. Our protocol for constructing Anderson towers allows for the direct numerical estimation of the contribution of individual eigenstates to broken-symmetry wave functions, which, to the best of our knowledge, was not done up to date for quantum antiferromagnets. In this respect, we would like to cite the results of Ref. [52], in which an analytic expression for the tower decomposition coefficients in the specific limit of the Bose-Hubbard model parameters is derived. Based on this, the authors show that one can find a signature of a nematic order when constructing the TOS for the quantum system being in the superfluid ground state of spin-1 bosons. Thus, it is instructive to implement our approach to explore canonical quantum antiferromagnets as well as other nontrivial magnetic orderings such as skyrmions.

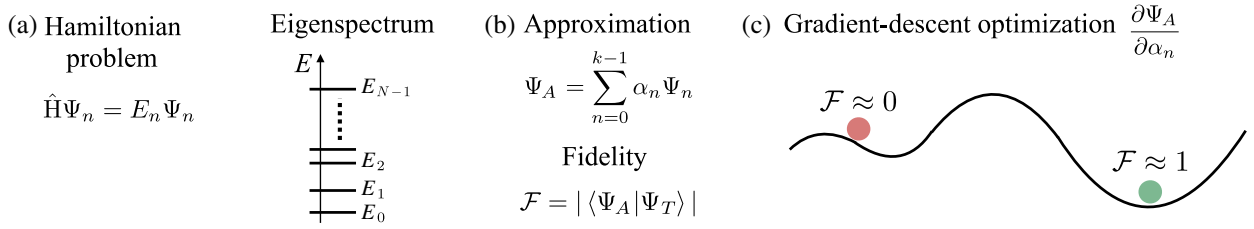

FIG. 2. Protocol for constructing Anderson's towers of states. (a) For the given Hamiltonian, one calculates a set of low-lying eigenstates. (b) On the basis of the calculated eigenstates, an initial approximation of the target state is prepared. The complex coefficients α_n are chosen to be random. (c) The coefficients are optimized within a gradient-descent approach aiming to maximize the fidelity between approximation and target wave functions. N is the corresponding number of energy levels.

B. Skyrmionic and antiferromagnetic TOS

The protocol presented above is general and can be applied for reconstructing classical orders stabilized with completely different microscopic mechanisms. To demonstrate this, we explore the TOS in antiferromagnets and skyrmionic systems that can be defined with the following general spin Hamiltonian:

$$\hat{H} = \sum_{ij} J_{ij} \hat{\mathbf{S}}_i \cdot \hat{\mathbf{S}}_j + \sum_{ij} \mathbf{D}_{ij} [\hat{\mathbf{S}}_i \times \hat{\mathbf{S}}_j] + \sum_i B \hat{S}_i^z. \quad (4)$$

Here, J_{ij} is the isotropic Heisenberg exchange interaction. $\mathbf{D}_{ij}$ is an in-plane vector that points in the direction perpendicular to the bond between neighboring i and j lattice sites and describes the Dzyaloshinskii-Moriya interaction (DMI). B is an external uniform magnetic field applied along the z direction. In the following, for constructing the skyrmionic towers, we use the parameters $J = -0.5$, $|\mathbf{D}| = 1$, and $B = 0.44$, which guarantee the stabilization of the quantum skyrmion wave function as the quantum ground state on a 19-site triangular-lattice supercell with periodic boundary conditions [45]. In turn, the exact diagonalization calculations of the antiferromagnetic systems with pure Heisenberg exchange ($J = 1$, $\mathbf{D} = 0$, and $B = 0$) are performed on the 4×4 square and 3×3 triangular supercells with periodic boundary conditions.

Following the developed protocol, we calculate a set of low-lying eigenstates for quantum Hamiltonians of the considered systems and then perform the optimization of the variational wave function with respect to the preselected classical order (target wave function). For the skyrmion problem, such a classical order represents a ground state magnetic configuration obtained for the corresponding classical Hamiltonian using the same set of model parameters as for the quantum counterpart. The low-energy part of the eigenspectrum presented in Fig. 3(a) is characterized by a sizable gap between the first 19 eigenstates and the rest of the spectrum. The optimization results show that the states at the bottom of the gap play a central role in reconstructing the coherent skyrmion state with Anderson towers and contribute about 80% to the probability of the resulting wave function. Basically, the obtained states structure agrees with the conventional picture of TOS [51], which suggests the emergence of the classical order from the degenerate ground state manifold of a quantum system. Exact diagonalization calculations show that the energy gap is controlled with the magnetic field and varies from 0.2 to 0.7 in units of DMI within the skyrmionic phase (Appendix A). Comparing this to the energy width of the set of 19 low-lying states that is about 0.03 in units of DMI, one can consider these eigenstates to be nearly degenerate. However, we additionally observe contributions to the tower from the excited states at the top of the gap. Such a deviation from the standard TOS scenario may be explained by the small size of the simulated systems.

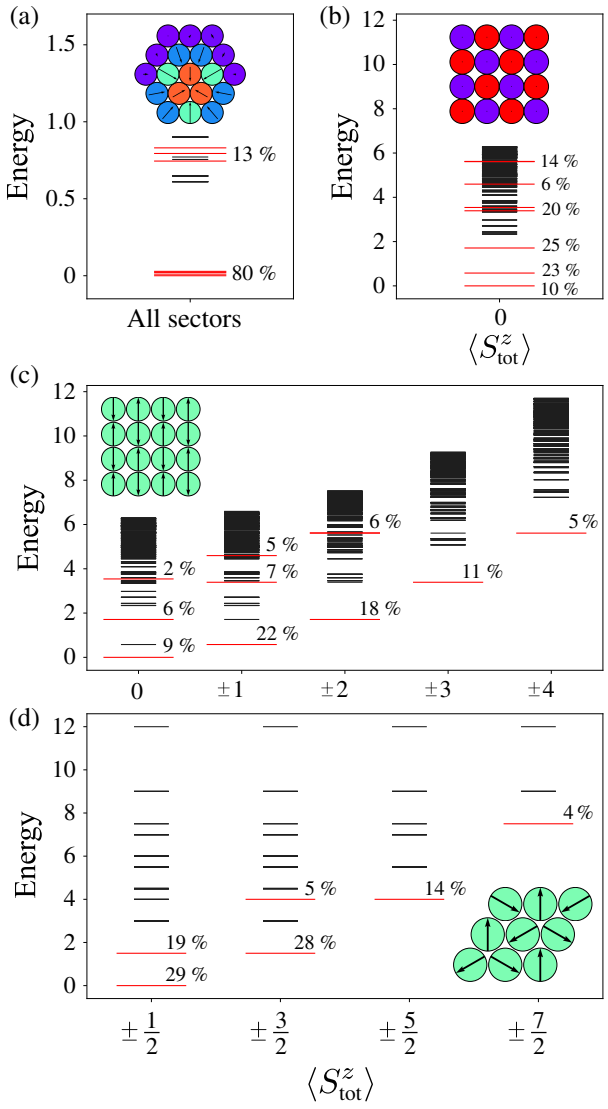

FIG. 3. Towers of states for skyrmions and antiferromagnets. Eigenspectra (black lines) and largest contributions to TOS (red lines) obtained for classical skyrmion (a), z-oriented AFM (b), y-oriented AFM (c), and 120° AFM (d) orderings. The simulations are performed with 19-site (a), 4×4 square [(b) and (c)], and 3×3 triangular (d) supercells. For the sake of the visualization, the eigenstates giving 1% or less contribution to the TOS are not highlighted in red.

The reconstructed classical skyrmionic order [inset in Fig. 3(a)] belongs to the class of topologically protected states of matter which are characterized by the nonzero value of a topological invariant. In the case of a discrete lattice, we consider the scalar chirality that plays the role of such an invariant and can be defined as follows for a specific wave function:

$$Q_\Psi = \frac{1}{\pi} \sum_{\langle ijl \rangle} \langle \Psi | \hat{\mathbf{S}}_i \cdot [\hat{\mathbf{S}}_j \times \hat{\mathbf{S}}_l] | \Psi \rangle, \quad (5)$$

where i, j, and l depict three neighboring spins that form an elementary triangular plaquette. We find that for all the TOS eigenstates the scalar chirality correlator is equal to about 0.55, and, as the result, the target wave function that corresponds to the classical order is characterized by the same Q_Ψ. This finding suggests a distinct explanation for the phenomenon of topological protection of classical skyrmionic structures. Accordingly, the nontrivial topological structure of the classical magnet is fully defined by a unique combination of the eigenstates of the corresponding quantum system. At the same time, each TOS eigenstate is featureless with respect to the any magnetization structure, which guarantees immunity and stability against an external magnetic influence.

Another important corollary of the TOS analysis of the magnetic skyrmions is that each TOS eigenstate can be represented as a linear superposition of trivial coherent states (tower of classical states) corresponding to the considered classical skyrmion and its replicas obtained applying translational and rotational symmetry operations:

$$|\Psi_n^{\mathrm{TOS}}\rangle = a_1 \left|\right\rangle + a_2 \left|\right\rangle + \ldots + a_{38} \left|\right\rangle . \tag{6}$$

Building from the same trivial wave functions, the TOS eigenstates differ from each other only in the values of the coefficients $\{a_1, \ldots, a_{38}\}$. Thus, by construction, the skyrmionic TOS contains redundant information on the topologically protected classical magnetic order, which suggests to see the TOS as an analog of the DNA molecules in the context of solid state matter. Appendixes A–C contain more information supporting these conclusions.

In the case of the square-lattice antiferromagnets, the target wave functions correspond to antiparallel Néel order. Figure 3 visualizes the contributions of the eigenstates to the Anderson towers for quantum antiferromagnets. If the directions of the magnetic moments in the classical texture are collinear to the z axis, all the nonzero contributions to the Anderson tower come from the states with zero total spin [Fig. 3(b)]. The nonmonotonic behavior as the energy of the state increases represents another peculiarity of the constructed tower. While the largest weights $|\alpha_n|^2$ are provided by the excited states belonging to the first and second eigenlevels, the ground state gives about 10% of the coherent state. If the classical antiferromagnetic structure is along the y axis, as shown in Fig. 3(c), the distribution of the leading contributions over spin sectors becomes completely delocalized in comparison with the z axis case. Such a tower is mainly built by the lowest-energy states in each spin sector. Similar to the quantum skyrmions, we additionally observe significant contributions from the excited states.

For the spin model (4) with the only nonzero antiferromagnetic interactions between nearest neighbors on a triangular lattice, the target coherent wave function corresponding to the classical order is assumed to be a 120° Néel state [53]. According to calculations on a 36-site cluster, the ground state of the quantum Heisenberg Hamiltonian on the triangular lattice is, as a consequence of frustration, only slightly ordered, if at all, as follows from the decay of the spin-spin correlation function at large interspin distances [54]. This frustration requires simulating quantum systems of large enough sizes in order to perform an extrapolation of the system's properties to the thermodynamics limit. Advanced techniques such as neural quantum state [55] potentially allow for modeling large quantum systems. However, they do not provide the required accuracy in determining the ground and the excited eigenstate energies of frustrated magnets [56], which makes it inevitable to use exact diagonalization methods.

Such fundamental limitations on the size of the frustrated systems encourage an active use of the TOS concept to explore the presence of magnetic order in the triangular-lattice Heisenberg antiferromagnet [32,57,58]. In particular, as shown in Ref. [32], there is a whole set of excited states which can constitute the tower of states. Our numerical results presented in Fig. 3(d) support this symmetry-based conclusion. For the in-plane 120° Néel ordering simulated with a 3×3 supercell, the eigenspectra resolved in total spin numbers is symmetrical. The largest contributions of about 29% of the target coherent wave function come from the ground eigenstates in spin sectors with $S^z_{\mathrm{tot}} = \pm\frac{1}{2}, \pm\frac{3}{2}$. It is clearly seen from Fig. 3(d) that the excited states of the same sectors provide non-negligible contributions from 5% to 19%.

Thus, one can define the candidate eigenfunctions that build the TOS with group-theoretical consideration or by using the gradient-descent approach we propose in this work. Importantly, our analysis of the quantum skyrmions and quantum antiferromagnets (Fig. 3) demonstrates that the coherent state representing the particular classical configuration can be reconstructed with only specific combination of the eigenstates. However, in the thermodynamic limit, following the original idea by Anderson, these states should collapse to the highly degenerate ground state manifold, which means that the quantum system in question can be described by an arbitrary superposition of the considered wave functions. Thus, one faces a critical problem that is not addressed in the previous works on TOS, namely, the mechanism responsible for the transformation of the random composition of the TOS eigenfunctions onto their specific combination. In the next section, we take a step forward and propose a concrete scenario describing such a transformation using the developed gradient-descent protocol.

C. Loss function for decoherence

The tower-of-states analysis is a very important approach to detect the spectral structure for several scenarios of

symmetry breaking in the thermodynamics limit, but it does not unveil all the details of such a transformation. To demonstrate this, we prepare 100 trial wave functions Ψ_R representing a random superposition of the TOS eigenstates (the corresponding eigenlevels are denoted with red in Fig. 3) for both square- and triangular-lattice quantum antiferromagnets. In other words, this random wave function is given by the following expression:

$$\Psi_R(\boldsymbol{\alpha}) = \sum_{n=0}^{k-1} \alpha_n \Psi_n^{\mathrm{TOS}}, \tag{7}$$

where α_n are random complex coefficients. One can think of constructing such random superpositions as a finite-size supercell imitation of the thermodynamics limit in which these TOS eigenstates should form a degenerate ground state manifold, which means that the quantum system can be found in an arbitrary combination of such eigenfunctions. For the square-lattice quantum antiferromagnet, we consider the case where TOS levels are in different S^z_{tot} sectors [Fig. 3(c)]. The eigenstates used to construct Ψ_R for the triangular-lattice Heisenberg model are collected from different spin sectors [Fig. 3(d)]. Magnetization textures obtained as a result of projective measurements of such random superpositions (Ψ_R) are presented in Figs. 4(a), 4(d). Triangular plaquette Heisenberg antiferromagnets are characterized by close to uniform magnetization profiles $\langle \hat{S}^z_i \rangle$ [Fig. 4(d)] with small random $\langle \hat{S}^x_i \rangle$ and $\langle \hat{S}^y_i \rangle$ components fluctuating from sample to sample. In turn, one can recognize an antiferromagnetic pattern in the case of the square lattice. However, the observed lengths of the magnetic moments are negligibly small compared to what one would expect for a classical configuration. These results raise an important question about the connection between Ψ_R and the coherent antiferromagnetic states $\Psi_{\mathrm{Néel}}$, which is not discussed in the previous works concerning the TOS, but at the same time it would be a demonstration of the internal consistency of the whole TOS theory, no more, no less.

It is also important to discuss details of building random skyrmionic TOS and compare them with coherent skyrmion wave function. As shown above, the eigenspectrum of the skyrmionic Hamiltonian (4) is characterized by 19 low-lying eigenstates that compose four eigenlevels and are well separated by a sizable energy gap from the rest of the spectrum [Fig. 3(a)]. The low-temperature physics of the quantum skyrmion system can be described by a random superposition of these 19 nearly degenerate eigenstates. Following the antiferromagnets consideration, we generate 100 different such superpositions and measure their scalar chirality. Remarkably, in all the cases, the total chirality (5) calculated for Ψ_R has the value of 0.51, which is also found for the ground state of the same Hamiltonian [45]. At the same time, the generated ensembles of Ψ_R in the case of skyrmions are characterized by featureless magnetization textures [Fig. 4(g)] fluctuating from sample to sample, which is similar to antiferromagnets.

Thus, the obtained picture of the magnetization density for the ground state of the quantum model clearly contradicts the results of real-space magnetization imaging experiments, such as spin-polarized scanning tunneling microscopy [49,59] and Lorentz transmission electron microscopy [60]. The magnetization densities obtained in these experiments in the case of ferromagnetic systems with Dzyaloshinskii-Moriya interaction at external magnetic fields are characterized by reproducible skyrmionic vortexlike profiles. In our case, such profiles are reproduced when solving the classical version of the quantum Hamiltonian [Eq. (4)]. Trying to harmonize the classical skyrmionic solution and quantum ground state with featureless magnetization, we arrive at the famous problem of the transition from the quantum realm characterized by a superposition of alternatives (outcomes) to the classical reality with a single outcome, which has haunted researchers since the very foundation of quantum mechanics [19,61,62]. However, the quantum-classical transition we deal with in this work is a specific one.

The performed numerical experiments on measurements of the magnetization density in skyrmionic systems and antiferromagnets unequivocally testify that there should be an additional transformation of the system's wave function before the measurement, which would give a classical spin configuration as outcome of the measurement. Now, we have to establish the relation of the TOS approach to the decoherence program [12–17]. First of all, according to the decoherence theory, macroscopic systems are never isolated from their environments, which automatically makes the TOS approach, which predicts the properties of an isolated quantum system in the thermodynamic limit, incomplete without taking into account the influence of the environment. The decoherence leads to the environment-induced superselection of states (pointer states), which remain stable in the presence of the environment. The environment has little effect on the pointer states, since they are already classical. Thus, following this definition, we would like to stress that the coherent (target) wave functions corresponding to the classical skyrmionic or antiferromagnetic textures we reconstruct within the TOS framework can be associated to such pointer states introduced in the decoherence theory. For simpler model situations, the transition from quantum singlet state to classical Néel state under the effect of the environment is studied in Refs. [63,64].

In general, the search for the pointer states can be realized within the following scheme. First, one has to define a general density matrix $\rho_{\mathcal{SE}}$ that describes an entangled superposition of the quantum system in question ($\mathcal{S}$) and the environment ($\mathcal{E}$). Then, it is necessary to compute the reduced density matrix for the quantum system by tracing the environmental part out: $\rho_{\mathcal{S}} = \mathrm{Tr}_{\mathcal{E}}\rho_{\mathcal{SE}}$. All possible states of the system are involved in $\rho_{\mathcal{S}}$ defined as a function of time.

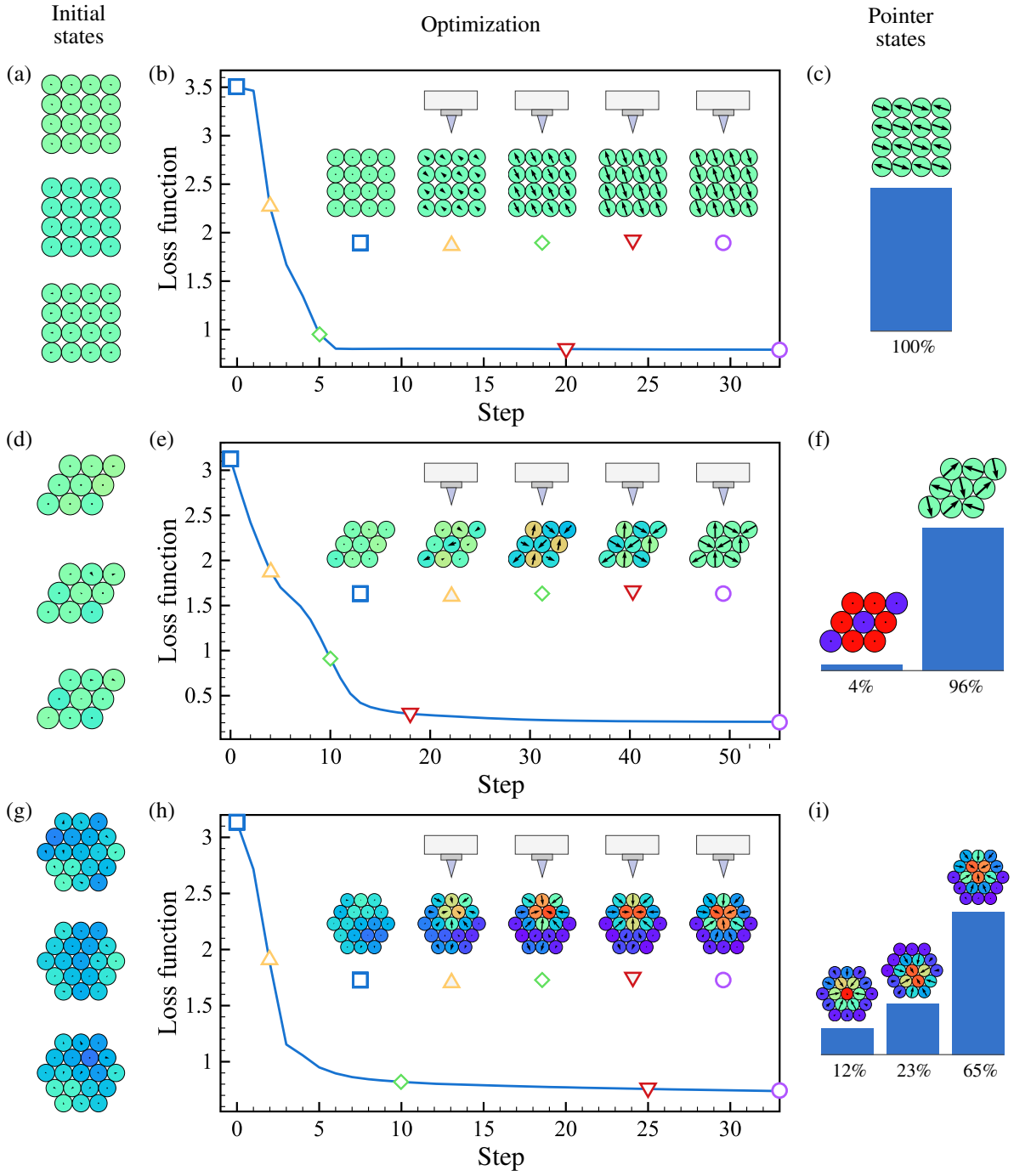

FIG. 4. Searching for pointer states. Examples of magnetic structures corresponding to the different realizations of the random state Ψ_R generated with TOS eigenfunctions in the case of square-lattice (a) and triangular-lattice (d) Heisenberg models as well as for quantum skyrmion (g). (b),(e),(h) Loss functions describing the decrease of the entanglement in the system in question due to decoherence. The insets show the evolution of the magnetic structures during the optimization. (c),(f),(i) Examples of pointer states—classical configurations that are preselected by the decoherence and revealed in the quantum state measurements. Histograms denote the percentage of realization of a certain pointer state in 100 independent numerical experiments for each spin model.

Thus, minimizing von Neumann entropy for $\rho_S(t)$ allows one to detect the pointer states. However, having introduced an environment explicitly, one would have to make some assumption on its properties, which leads to the loss of generality of the performed analysis. Besides, from the numerical point of view, a simulation of the environment to detect the pointer states looks somehow unrealistic, since it should be characterized by an exponentially larger number of degrees of freedom than those describing the investigated quantum system itself.

Fortunately, the wave functions we consider within the TOS theory to describe quantum antiferromagnets and skyrmions contain pointer states by construction. Thus, in our work, we mimic the influence of the environment on the quantum system by optimizing Ψ_R as a function of $\boldsymbol{\alpha}$ toward a coherent (pointer) state. In this way, the environment is taken into account on the level of a loss function without explicitly introducing it into the model. The discussion above on the decoherence theory makes the choice of the loss function obvious:

$$\mathbb{E}_A(\boldsymbol{\alpha}) = -\mathrm{Tr}\rho_A(\boldsymbol{\alpha})\log_2\rho_A(\boldsymbol{\alpha}), \tag{8}$$

where $\rho_A(\boldsymbol{\alpha}) = \mathrm{Tr}_B\rho_{AB}(\boldsymbol{\alpha})$ is the reduced density matrix for a half-system bipartition into parts A and B. This loss function is nothing but von Neumann entanglement entropy. Thus, in our consideration, the subsystem B acts like an "environment" in the sense of the set of degrees of freedom that are integrated out. As we show below, this procedure allows us to find a collection of few low-lying energy eigenstates which are closest to the classical analog. Their entanglement with "the surroundings" is minimal. This is consistent with the standard definition of pointer states but generates "the environment" in a much simpler and direct manner.

The use of such a loss function for optimizing Ψ_R allows us to describe the decrease of the uncertainty due to the contact of the quantum state with the environment. Some examples of the evolution of random states Ψ_R describing quantum antiferromagnets and skyrmions within gradient-descent procedure are presented in Figs. 4(b), 4(e), and 4(h). Depending on the initial random combination of the TOS eigenfunctions, different alternatives of the classical outcome can be realized. In the case of the square-lattice Heisenberg antiferromagnet, the symmetry of the TOS eigenstates allows for the formation of only one type of pointer state, that is, the 180° Néel configuration [Fig. 4(c)]. At the same time, there are two alternatives allowed by the symmetry of the triangular-lattice Heisenberg model, namely, 120° Néel and collinear stripe phases [Fig. 4(f)]. The latter is characterized by a larger energy than the former one for the considered spin Hamiltonian (4). However, including next-nearest-neighbor exchange interactions in the model Hamiltonian is known to change the balance between these classical configurations [65].

The survival of the most robust, that is, pointer states, in an environment was called by Zurek "quantum Darwinism" [17]. It is worth to mention that the word "Darwinism" when discussing an optimization problem means probably much more than just a bright analogy. Formal correspondence between Darwinian evolution, the optimization problem in machine learning, and statistical mechanics was recently discussed in Refs. [66,67]; the loss function corresponds to (minus) the logarithm of fitness in evolutionary biology and to the free energy in statistical mechanics.

D. Scenario for experiments

The theory of quantum Darwinism for degenerate states presented above describes the environment-driven evolution of the eigenfunction of a system, which allows one to establish a direct connection between entangled quantum states and known classical magnetic orders observed for some crystalline systems. To extend this analysis, we show that our approach can reveal pointer states unknown before, which will encourage new experiments. For these purposes, we consider the antiferromagnetic Heisenberg spin-$\frac{1}{2}$ model defined on the perfect triangular plaquette [Fig. 5(a)]. This model can be realized with different experimental techniques such as ultracold atoms in optical lattice [68,69], photonic quantum simulators [70], or scanning tunneling microscopy. This system is characterized by a fourfold degenerate ground state that is separated from the excited states by a spin gap of $3J/2$ [Fig. 5(a)].

We are interested in describing the ground state of this quantum system, which means that the corresponding experimental temperature should be smaller than the spin gap. Because of the ground state degeneracy, the system is characterized by random orientations of spins of random lengths. It strongly differs from the classical 120° antiferromagnetic state for which the length of the spin is $\frac{1}{2}$. Moreover, the quantum and classical solutions are different in entanglement. While for the former the von Neumann entropy averaged over single-site subsystems can be estimated to be about 0.78, the classical solution corresponds to the trivial coherent state with zero entanglement entropy. Our aim is to find pointer states—combinations of ground states that are characterized by the smallest entanglement.

To find the pointer wave functions for the Heisenberg triangle quantum states, we adopt the loss function

$$\mathbb{E}_\Delta(\boldsymbol{\alpha}) = \frac{1}{3}[\mathbb{E}_A(\boldsymbol{\alpha}) + \mathbb{E}_B(\boldsymbol{\alpha}) + \mathbb{E}_C(\boldsymbol{\alpha})] \tag{9}$$

that represents the average value over the loss functions calculated with Eq. (8) for sublattices A, B, and C. The resulting pointer quantum states [an example is presented in Fig. 5(c)] are characterized by a von Neumann entanglement entropy of 0.65 for each single-site subsystem. This is the minimal value that can be reached for the given ground state manifold. Such states reveal 120° antiferromagnetic order. However, in comparison with the classical ordering, the magnetic moments are reduced in the pointer state. The length of the ith spin in the state Ψ_A can be calculated as $\sqrt{\langle\Psi_A|S_i^x|\Psi_A\rangle^2+\langle\Psi_A|S_i^y|\Psi_A\rangle^2+\langle\Psi_A|S_i^z|\Psi_A\rangle^2}$ and is equal to 0.33, while the classical spin length is $\frac{1}{2}$. Therefore, the pointer states that fulfill our criterion of minimal entanglement can be classified as hybrid and reveal both quantum and classical properties.

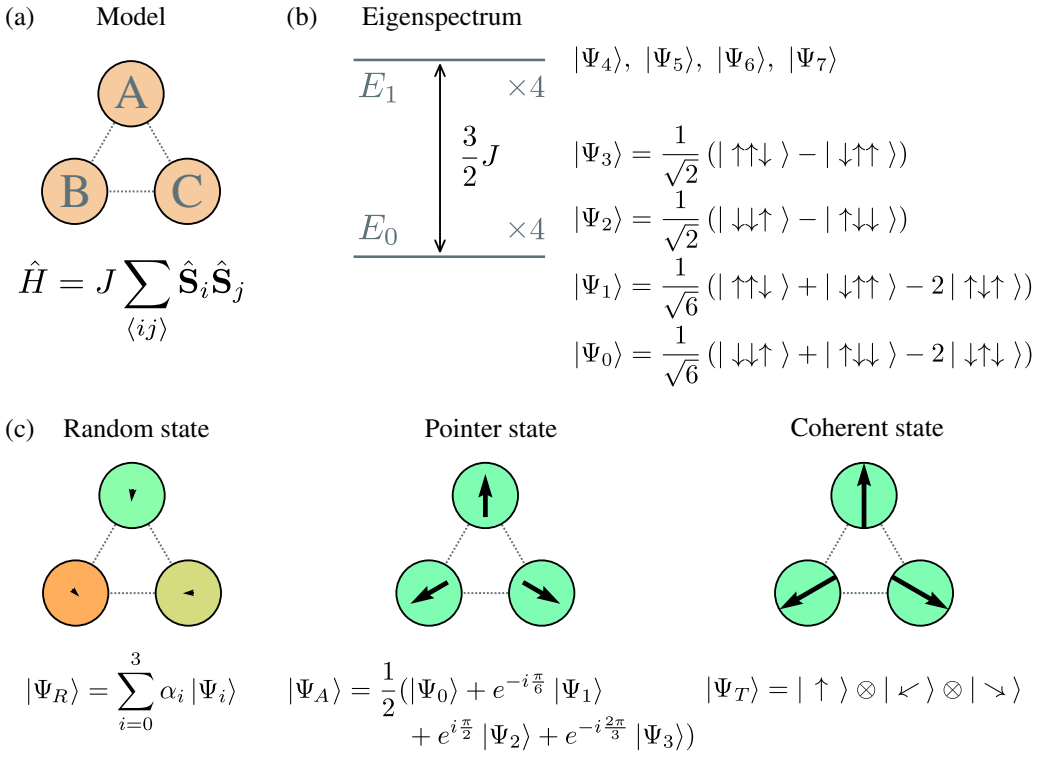

FIG. 5. Candidate for demonstrating the quantum Darwinism of degenerate quantum systems in real experiments. (a) Antiferromagnetic Heisenberg model defined on the triangular plaquette. (b) Eigenspectrum of the Heisenberg model characterized by fourfold degenerate ground and excited states. (c) Example of a magnetic structure corresponding to a random superposition Ψ_R of ground eigenstates, pointer state Ψ_A optimized with respect to von Neumann entropy showing reduced local magnetization, and classical model solution Ψ_T.

The noncollinear spin ordering of the pointer states should facilitate their detection in real experiments. In this regard, we believe that an appropriate experimental platform to realize the Heisenberg-triangle model is provided by ultracold atoms in optical lattices. In these experiments, the basic system's parameters—the tunnel matrix elements, a potential bias, and on-site interaction energies—can be tuned in such a way as to mimic many-body spin Hamiltonians including the isotropic Heisenberg model with antiferromagnetic as well as ferromagnetic couplings [68]. Examples of experimental results that could be relevant for confirming the quantum Darwinism model on the degenerate states include a realization of three Ising spins on a frustrated triangular cluster [71], a demonstration of antiferromagnetic superexchange interactions in ultracold atomic dimers [69], or the simulation of noncollinear orders [72] among others. Importantly, there also are techniques for probing the entanglement in ultracold atomic systems [71], which is crucial for characterizing the hybrid states we predict.

The other option is to study clusters of magnetic adatoms at metallic surfaces; in the simplest geometry, this can be just magnetic dimers. As shown theoretically in Ref. [63], the state of such a dimer has a phase transition from a quantum singlet state to a classical antiferromagnetic state when the ratio of the hybridization parameter with a fermionic bath to the interatomic hopping increases so that one goes from an isolated quantum system to an open one. The conduction electrons in the metallic substrate play the role of the fermionic bath. The magnetic state of individual atoms can be probed by spin-polarized scanning tunneling microscopy [73], and the above-mentioned ratio can be changed in two ways. First, one can use different thicknesses of isolating spacer between the adatoms and the substrate using, for instance, atomic terraces at the spacer, for the same interatomic distances. Alternatively, and probably even simpler, one can put atoms at different distances for the same substrate. Such experiments look quite straightforward and practically doable.

III. DISCUSSION AND OUTLOOK

In our work, we reveal and explore a connection between quantum and classical systems with the combination of the Anderson tower of states and decoherence theory. On the examples of topologically protected skyrmionic systems and of the antiferromagnet, we unambiguously show that the classical spin order can be reconstructed only from a specific set of a few low-lying eigenstates of the corresponding quantum Hamiltonian. Reconstruction with TOS assumes the degeneracy of the states that form each tower, which can be realized either on the level of small-size

quantum systems as in the case of the skyrmions or in the thermodynamics limit (antiferromagnets). The original TOS theory does not explain the mechanism that promotes the classical combinations among an infinite number of other superpositions that can be found within a degenerate manifold. We answer this question and show that the decoherence induced by a quantum environment plays a decisive role in the specific choice in favor of a classical state of a system which is *a priori* quantum.

The demonstrated reconstruction of pointer states from the tower of states by just minimizing the entanglement entropy in that subspace could have interesting applications in identifying the order in systems where one knows that there is a phase transition but has no clue as to what the order could be (a problem known as hidden order): From the low-energy states, one could try to determine the linear combinations with lowest entanglement and see if some kind of classical order appears in the resulting state.

Regarding its technological implications, we note that each TOS wave function encodes multiple copies of the same classical order and, at the same time, is featureless on the level of the magnetization density. It means that such a quantum representation of the classical order guarantees maximal protection of the information against different defects or external fluctuations. In this case, the information is encoded in a very sophisticated way in entangled states of a quantum system, which requires the involvement of an extremely powerful decryptor. As we show in this work, the quantum environment facilitates the solution of this decoding problem and prepares the state to read out by an observer. This looks promising for the realization of a quantum search system in which information is retrieved through the contact of a carefully prepared quantum system with a quantum environment that is characterized by an exponentially large number of degrees of freedom. It suggests an alternative to Grover's search algorithm [74] based on amplifying the amplitude of the concrete basis function for isolated quantum systems. Thus, we believe that the proposed combination of the TOS and decoherence theory can be employed to solve not only fundamental problems in condensed matter physics as demonstrated in this paper, but also more practical ones related to the development of quantum technologies.

Codes for constructing the tower of states and examples of reconstructing the Néel orders on a 3×3 triangular supercell have been deposited in Zenodo [75].

ACKNOWLEDGMENTS

We thank Andrey Bagrov and Tom Westerhout for useful discussions. We also thank an anonymous referee for very insightful comments on the connection between our results and the standard theory of pointer states. This work was supported by the Swiss State Secretariat for Education, Research and Innovation (SERI) under Research Preparation Grants with Russia 2020, the project Quantum skyrmions. V. V. M. and O. M. S. also acknowledge the support from the Russian Roadmap on Quantum Computing (Contract No. 868-1.3-15/15-2021). The work of M. I. K. was supported by the European Research Council (ERC) under the European Union's Horizon 2020 research and innovation program, Grant Agreement No. 854843-FASTCORR. The work of E. A. S. was supported by the European Union's Horizon 2020 Research and Innovation program under the Marie Skłodowska Curie Grant Agreement No. 839551-2DMAGICS. Exact diagonalization calculations were performed on the Uran supercomputer at the IMM UB RAS.

APPENDIX A: TOS FOR SKYRMIONS

In this section, we discuss the structure of the eigenspectrum and analyze different approximations of the classical skyrmion order obtained with TOS protocol. Figure 6(a) gives an enlarged view on the low-energy part of the spin Hamiltonian eigenspectrum and demonstrates important features related to its structure and degeneracy, which supplements data presented in Fig. 3 in the main text. One can see that the width of the level band at the bottom of the energy gap is much smaller than the size of the gap, which confirms our consideration assuming the degeneracy of these states. The energy gap value is larger than 0.2 within the skyrmionic phase [Fig. 6(b)].

In our work, we construct various towers of states that differ from each other in the number of involved eigenlevels and corresponding eigenstates. The example of the typical loss-function behavior during the optimization process is given in Fig. 6(c). It demonstrates a steep decrease for $N < 20$, where N is the number of eigenlevels taken into account. Further increasing N leads to the saturation of the loss function. Importantly, the number of eigenstates we consider is negligibly small with respect to the total dimension of the Hilbert space. More specifically, while the total dimension of the Hilbert space is equal to 2^{19}, to construct an approximation of the coherent skyrmion state we use superpositions of up to 495 eigenstates that can be packed into 105 different eigenlevels taking into account the degeneracy of the eigenfunctions.

Figure 6(d) shows the comparison of the probabilities of the basis functions that give the largest contribution to the quantum skyrmion and to the coherent skyrmion state and its approximations with different numbers of N. The probability function for Ψ_T is characterized by a steplike profile, which means that this quantum state is highly structured in the Hilbert space. By contrast, the quantum skyrmion is strongly delocalized. Figure 7 shows the composition for some approximations of the coherent skyrmion state. The largest weights ($\sum_n \alpha_n^2$, where n corresponds to a particular eigenlevel) are provided by degenerate states corresponding to the first three excited energy levels. The eigenstates of larger energies give much smaller contributions, but they are important to reach the

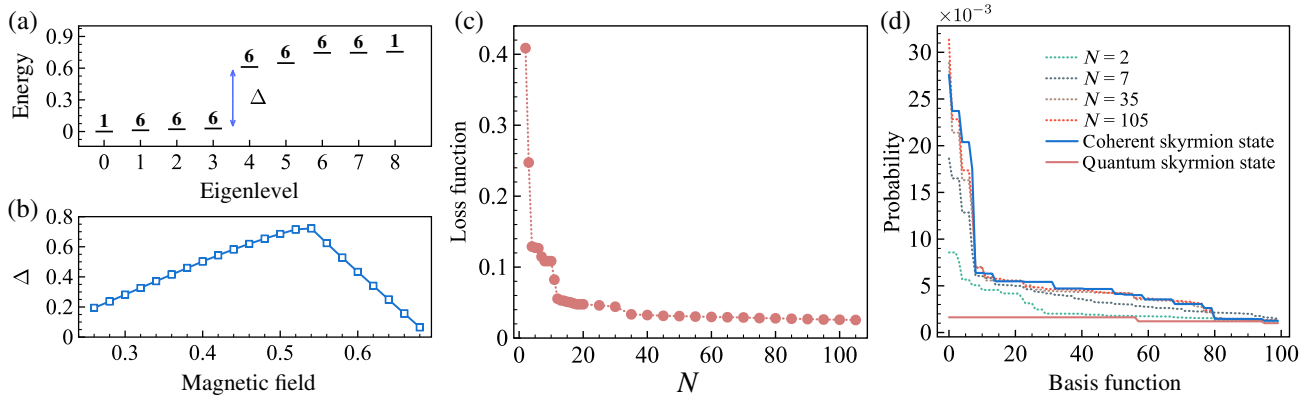

FIG. 6. Structure of the eigenspectrum and performance of the gradient-descent optimization in the case of the skyrmionic TOS. (a) Low-energy part of the eigenspectrum of the quantum Hamiltonian, Eq. (4) obtained with $J = -0.5$, $|\mathbf{D}| = 1$, and $B = 0.44$. The numbers denote the degeneracy of each eigenlevel. (b) Magnetic field dependence of the energy gap between the low-lying eigenlevels and the rest. (c) Dependence of the loss function on the number of eigenstates of minimal energy. (d) Comparison of the ordered distributions of quantum states amplitudes. Only the hundred basis functions giving the largest contribution to the particular state are considered.

high fidelity in reproducing the concrete solution of the classical version of the Hamiltonian (4). Indeed, as can be seen from Fig. 8, the local magnetization of the quantum Hamiltonian (4) is uniformly distributed on the lattice. We find that already the first approximation for Ψ_A that takes into account a small number N of levels leads to a magnetization profile that reminds one of the classical skyrmion spin texture. Such an approximation is formed with the ground state and the sixfold degenerate first excited state. Further extension of the set of excited states increases the fidelity between the target wave function Ψ_T and its approximation Ψ_A. For $N = 105$, the fidelity reaches the value of 97.5%.

For a complete characterization of the transition from the quantum skyrmion wave function to the classical skyrmion

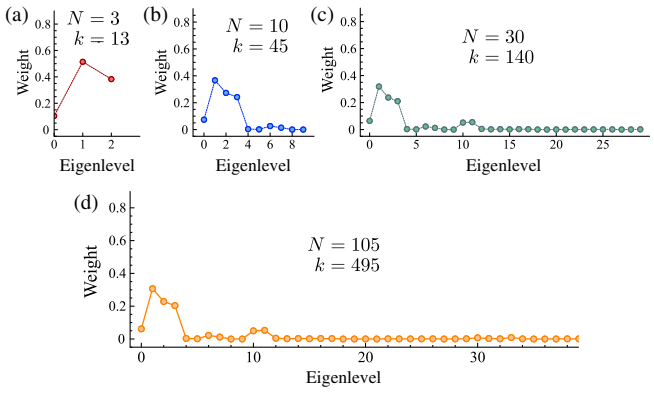

FIG. 7. Structure of the coherent skyrmion state approximations. Results obtained with different numbers of states from the low-lying part of the eigenspectrum of the Hamiltonian Eq. (4). The points denote the sum of probabilities (α_n^2) of the eigenstates corresponding to the same energy (eigenlevel). N denotes the number of eigenlevels with different energies.

state, the performed investigation of the magnetization pattern should be supplemented by the calculation of the scalar chirality, Eq. (5), and its distribution over the system in question [45], contributions of the individual triangles. We note that if the Hamiltonian (4) is defined on an infinite lattice, the problem can be solved on the basis of a supercell with periodic boundary conditions, and all individual triangular plaquettes produce the same contribution to the total chirality. The distribution of the chirality is, thus, uniform as the distribution of the magnetization in the system. As the bottom row in Fig. 8 shows, in the case of the classical skyrmion state Ψ_T and its different approximations Ψ_A, the scalar chirality has a nonuniform distribution with the largest contributions from the triangles characterized by the strongest variation of the magnetization, which can be explained by the smallness of the system. Importantly, the values of the total chirality are in the range 0.52–0.56 within the series of approximations as well as for the target wave function Ψ_T that corresponds to the classical skyrmion structure.

Recent experiments [76] show the possibility of stabilizing antiskyrmions on an equal footing with ferromagnetic skyrmions in a cubic chiral magnet. Thus, searching for a superposition of the quantum eigenstates that reconstructs antiskyrmion and comparison with the skyrmion TOS could represent next interesting problems to explore with our theory. As a preliminary step for future considerations, we define coherent states corresponding to antiskyrmionic counterparts for three ferromagnetic skyrmions considered in our work. Then, by using the developed optimization procedure, we construct Anderson towers of the 495 low-lying eigenstates to get the best approximation for the classical antiskyrmion orderings. In contrast to the skyrmion case, for which the same set of eigenfunctions gives the fidelity of 97.5% between the coherent state and

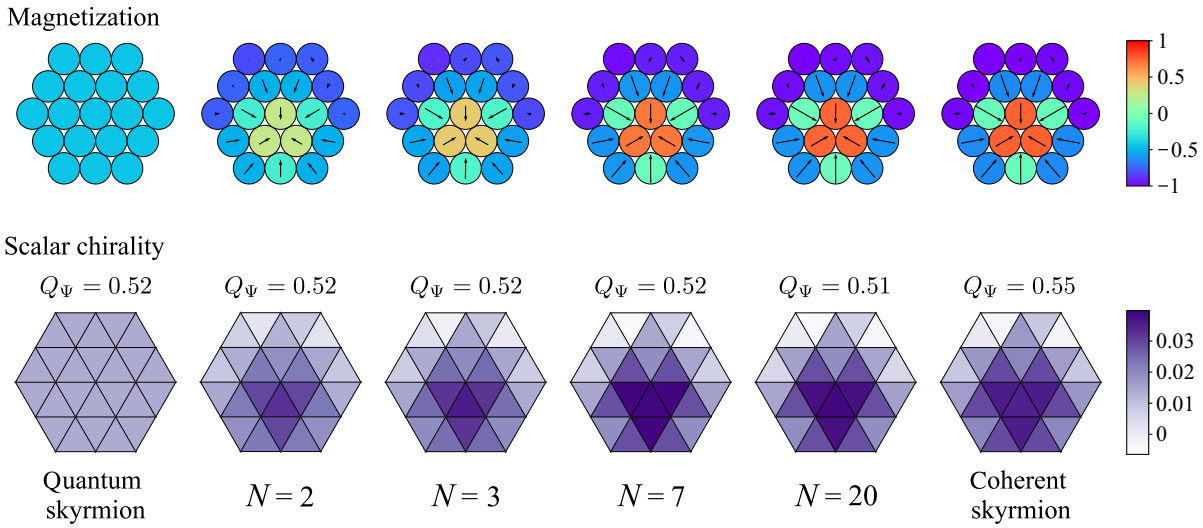

FIG. 8. Magnetization (top) and scalar chirality (bottom) calculated for the reconstructed wave function corresponding to the classical skyrmion with different numbers of eigenstates of the parent spin Hamiltonian. The arrows denote the in-plane direction of spins, while the z components are defined with color. The triangle-resolved scalar chirality Q^{Ψ}_{ijl} denoted with shaded triangles is calculated for a real quantum skyrmion state (left plaquette), a coherent state with classical profile of the magnetization (right plaquette), and for quantum states that are different approximations of the classical skyrmion within the Anderson tower approach. N denotes the total number of low-lying energy levels involved in the state reconstruction.

its approximation, the reconstruction of the antiskyrmions is characterized by a very low fidelity that is not higher than 16%. It suggests that the skyrmion and antiskyrmion TOS may belong to different parts of the eigenspectrum of the periodic two-dimensional quantum system. To clarify this, high-energy excited states should be investigated, which is a complex computational problem beyond the scope of this study.

From the technological perspective, it is of tremendous interest to move skyrmions by an applied spin-polarized in-plane electron current or by pulses of magnetic fields introduced by AFM tips. Importantly, in such investigations, one deals with isolated magnetic skyrmions that are normally stabilized in finite working areas with open boundaries. Oppositely, in our work, we explore properties of infinite magnetic systems that are simulated by means of supercells with periodic boundary conditions. In other words, we imitate a lattice of quantum skyrmions, which prevents one from describing a driven isolated quantum skyrmion in the present setup. Nevertheless, one could model a nonequilibrium dynamics of the quantum skyrmion lattice that is generated by laser pulses. Generally, such simulations require account of excited states of the quantum model above the gap. It means that a further development of efficient exact diagonalization techniques is needed as in the case of the antiskyrmions simulations described above.

APPENDIX B: ONE TOWER FOR DIFFERENT PHASES

The results presented in the main text and Appendix A justify the possibility to relate the eigenspectrum of the quantum spin Hamiltonian (4) to the classical order obtained for the particular value of the interspin interaction and the magnetic field. In this section, we demonstrate the power of the proposed approach in imitating different trivial (spin spiral) and nontrivial (skyrmion) topological structures, simultaneously. For this purpose, we consider the same set of $k = 495$ eigenstates obtained for the quantum model with the parameters $J = -0.5$, $|\mathbf{D}| = 1$, and $B = 0.44$. Some examples presented in Fig. 9 confirm

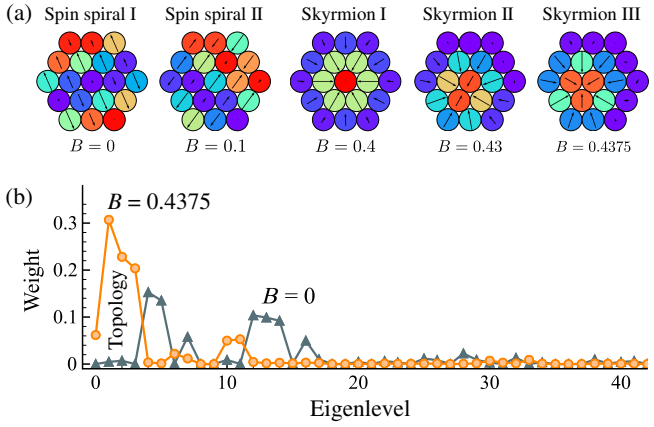

FIG. 9. Reconstruction of different phases. (a) Examples of classical spin spiral and skyrmion magnetic configurations stabilized at different magnetic fields B that can be reproduced with high fidelity, $\mathcal{F} = 0.95$, 0.96, 0.97, 0.97, and 0.97 (from left to right) by using the eigenspectrum of the quantum Hamiltonian (4) with the fixed set of model parameters $J = -0.5$, $|\mathbf{D}| = 1$, and $B = 0.44$. (b) Comparison of the contributions to approximations of the spin spiral ($B = 0$) and skyrmion ($B = 0.44$) configurations.

the high fidelity of the reconstruction of completely different coherent states with the same set of quantum states. Surprisingly, we find that coherent states corresponding to topologically trivial and nontrivial classical configurations can be obtained with the same set of 495 eigenfunctions of the quantum spin Hamiltonian (4) that reveals the quantum skyrmion state. The comparison of the contributions to the corresponding approximations of the classical spin spiral and skyrmion configurations is presented in the bottom in Fig. 9. These two profiles are clearly different, and one can conclude that the topology of a classical spin texture is related to the first few ($N = 1$, 2, and 3 excited) levels of the quantum spectrum.

As follows from Fig. 9, one can distinguish the spin spiral and skyrmion phases by the decomposition of the weight profiles of the towers. In general, performing phase classification in the case of noncollinear magnets is supposed to be a hard problem that can be solved by inventing order parameters or other means including machine learning [77–80]. Our results suggest a distinct way for phase classification through Anderson towers.

APPENDIX C: TOWER OF CLASSICAL STATES

The main focus in this paper is on reproducing the classical state with low-lying quantum states, and one might think that the quantum-classical connection in the Anderson's approach works only in one way. However, it is not the case. A simple justification can be demonstrated, for example, for the antiferromagnetic configuration of two spins $S = \frac{1}{2}$. On one hand, the antiferromagnetic state can be expressed through a combination of the singlet wave functions $\Psi_{A_1} = (1/\sqrt{2})(|\uparrow\downarrow\rangle - |\downarrow\uparrow\rangle)$ and $\Psi_{A_2} = (1/\sqrt{2})(|\uparrow\downarrow\rangle + |\downarrow\uparrow\rangle)$, which corresponds to the tower of quantum states. On the other hand, the singlet wave function entangles two coherent antiferromagnetic states $\Psi_{T_1} = |\uparrow\downarrow\rangle$ and $\Psi_{T_2} = |\downarrow\uparrow\rangle$. It means that one can construct two different types of towers: the tower of the classical states to reproduce the quantum state and, vice versa, the tower of quantum wave functions to reconstruct the antiferromagnetic classical configuration. Thus, Anderson's approach supports both classical-quantum and quantum-classical channels of characterization of the system, which fundamentally distinguishes this approach from measurement-based theories that assume complete or partial collapse of the quantum wave function upon measurement.

To explore the possibility of reconstructing the quantum states, which are the eigenfunctions of the quantum spin Hamiltonian, with classical solutions, we built a tower of coherent states on the basis of the classical skyrmionic solution obtained at $B = 0.44$. This magnetic skyrmion is visualized in Fig. 9(a) (skyrmion III), and its properties regarding the spin-spin correlation functions are discussed in a previous work [45]. Initially, the tower of states is built up as a random superposition of the coherent states corresponding to the considered classical skyrmion and its replicas obtained applying translational and rotational symmetry operations as visualized in Fig. 10(a). The number of coherent states contributing to the tower depends on the specific classical configuration and in our case is equal to 38:

$$|\Psi_{\mathrm{A}}^{\mathrm{cl}}\rangle = a_1 \left|\right\rangle + a_2 \left|\right\rangle + \ldots + a_{38} \left|\right\rangle , \tag{C1}$$

where a_i is the amplitude of the ith coherent state. One should note that $\sum_i a_i^2 \neq 1$, since coherent states in

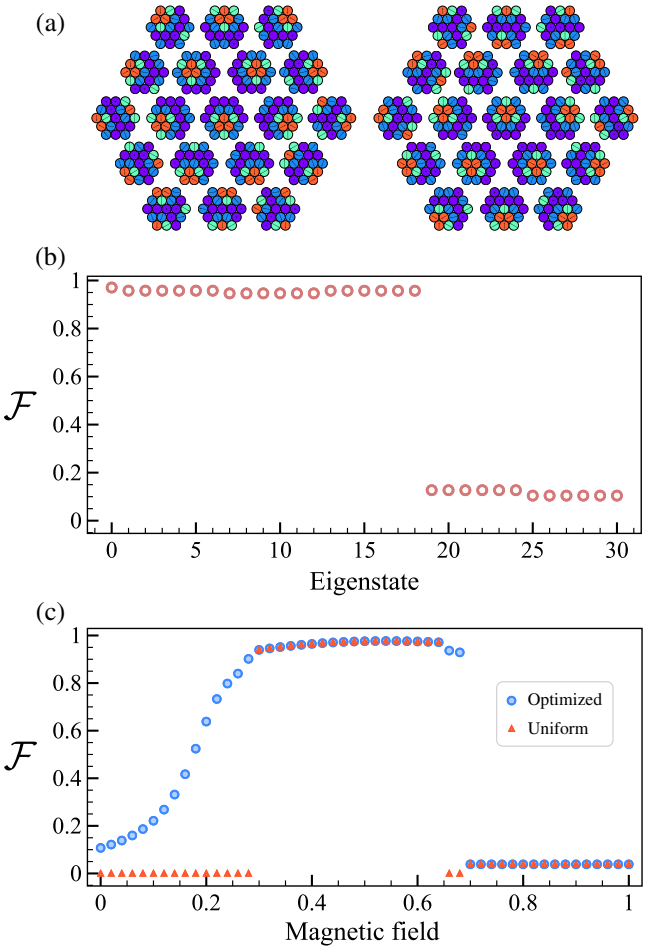

FIG. 10. Tower of classical skyrmions. (a) 38 classical skyrmionic configurations obtained at $B = 0.44$ and used to define the tower of classical states [Eq. (C1)]. (b) Reconstruction fidelities of the ground and excited eigenfunctions of the quantum Hamiltonian [Eq. (4)] calculated at B = 0.44. The reconstructions are performed with optimization of the tower of classical states [Eq. (C1)]. (c) Calculated fidelities (circles) describing the quality of optimizing the quantum ground states at different magnetic fields with the tower of classical states. Triangles correspond to the approximation of Eq. (C1) taken with $a_1 = a_2 = \cdots = a_{38} = 0.1078068$.

Eq. (C1) are not orthogonal to each other. Nevertheless, the state Ψ_A^{cl} remains to be normalized to 1 in the σ^z basis.

The constructed tower is optimized with the gradient-descent approach to get maximum possible overlap with one of the states from the low-lying part of the eigenspectrum. For demonstration purpose, we choose the eigenspectrum of the quantum spin Hamiltonian (4) calculated for the same value of the magnetic field $B = 0.44$. From Fig. 10(b), one can see that the constructed classical tower reveals high fidelity (more than 95%) in reconstructing the eigenstates with $k = 0, \ldots, 18$ that belong to the low-energy part of the eigenspectrum below the energy gap. In contrast to the low-energy eigenfunctions, the calculated fidelities for the excited states above the gap are nearly zero.

The optimization of the quantum ground states obtained at different values of magnetic field [circles in Fig. 10(c)] reveal high fidelities close to 1 within the skyrmionic phase for $0.3 \leq B < 0.66$ [45]. Interestingly, for $B < 0.3$, one can find a combination of coefficients in Eq. (C1) with the gradient-descent method such that there is a nonzero overlap between the quantum ground state and the constructed tower of classical skyrmionic configurations. Even at $B = 0$, the fidelity is not identically zero and has the value of about 0.1, which is direct evidence that there is a quantum superposition of the spin spiral and skyrmion states in the range of fields $0 \leq B < 0.3$.

Another important result is that the optimized coefficients within the skyrmionic phase ($0.3 \leq B < 0.66$) are practically the same for each term in Eq. (C1). Triangle symbols in Fig. 10(c) denote the overlap between the quantum ground state calculated for a specific magnetic field and the wave function Ψ_A^{cl} taken with $a = a_1 = a_2 = \cdots = a_{38} = 0.1078068$. One can see that, using such a uniform state

$|\Psi_U^{\mathrm{cl}}\rangle = a\Big(\Big|$ 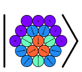 $\Big\rangle + \Big|$ 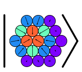 $\Big\rangle + \cdots + \Big|$ 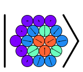 $\Big\rangle \Big),$ (C2)

we can approximate any ground state within the skyrmionic phase with high fidelity. In other words, it means that the quantum ground state within the skyrmionic phase is almost insensitive to the external magnetic field. This specific choice of coefficients gives the wave function for a pure skyrmion state, so fidelity of this pure skyrmion state with the state that is a superposition of spin spirals and skyrmions is zero, as we see for $B < 0.3$.

Thus, a highly entangled wave function $|\Psi_0\rangle$, the ground state of the quantum spin Hamiltonian (4), can be expressed as a simple superposition of trivial coherent states that correspond to the same classical magnetic configuration and differ from each other only by translation or rotation operations. We believe that this result is remarkable. First of all, it directly demonstrates the connection between quantum and classical skyrmion states. Previously, the relation between quantum and classical skyrmionic solutions was established only on the level of observables, such as the magnetization, the spin structural factors, and the scalar chirality. Furthermore, Eq. (C1) suggests a distinct way for simulating and storing large-scale quantum topological states. They can be efficiently prepared on the basis of the classical solution, thus avoiding the hard-to-do exact diagonalization procedure, for which the current limit is a quantum system of 50 spins [81].

It is also worth discussing the connection of the quantum state decomposition onto coherent states realized within Eq. (C1) and the results of projective measurements of Ψ_0 reported in our previous work [45]. Looking at Eq. (C1), one might think that one of the classical replicas of a skyrmion should be observed in the experiments after the measurement. However, it is not the case. A single projective measurement in σ^z basis results in a basis function that can be attributed to one or more coherent states (1) simultaneously. That is why in Ref. [45] when measuring Ψ_0 a sequence of basis states that are fully unstructured with respect to the classical skyrmion profile is observed. Averaging over such measurements leads to a uniform magnetization. To amplify the contribution of one particular coherent state, it is necessary to perform the measurements by using the corresponding local bases for each spin in the system. In principle, such a procedure can be realized in quantum computing. In this case, one gets the basis state $|000\ldots0\rangle$ or $|\uparrow\uparrow\uparrow\ldots\uparrow\rangle$ with the probability approximately 0.01, which can be considered as a finite value in comparison with practically zero contribution of that basis function in the global σ^z basis.

A purely quantum mechanism that allows one to preselect a specific coherent state from Eq. (C1) before the measurements is discussed in Sec. II C in the main text.

APPENDIX D: ADDITIONAL ANALYSIS OF THE POINTER STATES SEARCH

In this section, we extend the discussion presented in Sec. II C in the main text. The periods of the square- and triangular-lattice antiferromagnetic structures considered in this work are shorter than that of the skyrmion one. The square 4×4 and triangular 3×3 supercells we use can be safely divided into smaller fragments (clusters) locally reproducing the corresponding antiferromagnetic configuration between nearest spins. It means that the reduced density matrix introduced in Eq. (8) is defined on the system's fragment that is expected to contain complete information on the magnetic configuration stabilized in the classical case. For the quantum skyrmion system, the situation is more complicated. A 19-site plaquette can host only one skyrmion [45]. It means that the subsystem A of nine sites for which we calculate ρ_A covers roughly half of the skyrmion in the classical case. Judging by the fact that the optimization of entanglement entropy calculated for the local fragment of the quantum system restores the classical skyrmionic structure, one can conclude that the

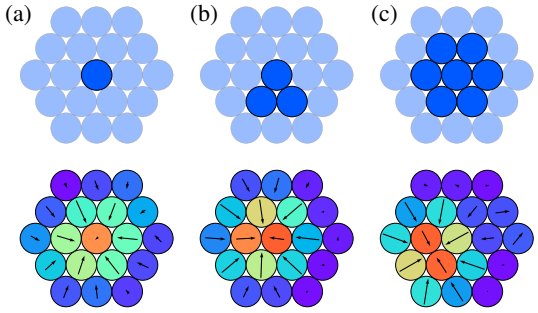

FIG. 11. Comparison of the optimization results obtained with different numbers of spins in the subsystem A [Eq. (8)] used to extract information on entanglement of the system in question. In the top, the spin clusters used for the definition of the reduced density matrix ρ_A in the optimization procedure Eq. (8) are highlighted. The bottom gives examples of the resulting skyrmionic structures induced by the minimization of the entanglement entropy defined for the corresponding clusters.

corresponding reduced density matrix compresses the complete information on this three-dimensional topological texture.

To elaborate on this point and to probe the limit of such quantum compression of the classical information, we perform the quantum-classical optimization described in Eq. (8) by choosing subsystems of different shapes and different numbers of spins involved in the reduced density matrix. It follows from Fig. 11 that the symmetry and size of the subsystem used to probe the entanglement strongly affect the quality of the resulting classical state. Nevertheless, even the single-site entropy contains enough information to get a recognizable skyrmionic pattern, albeit with some symmetry distortion.

In the proposed realization of the Anderson idea on tower of states, one can find a motif of generative machine learning [82], one of the goals of which is to generate new reliable content (images and videos). Instead of explicitly specifying a target state, we can describe its required properties using an appropriate loss function. Importantly, such properties can be related not only to some physical observables (magnetization and spin-spin correlation functions), but also to pure theoretical physical quantities such as von Neumann entropy. It opens the way to constructing different classical states as well as various quantum-classical hybrid wave functions characterized by nonzero entanglement and specific magnetization patterns.

APPENDIX E: EXACT DIAGONALIZATION DETAILS

The eigenstates used for the calculation of the scalar chirality and magnetization are obtained via an exact diagonalization approach. For that purpose, we use the implicitly restarted Arnoldi algorithm as implemented in the ARPACK library. Such a solution allows us to optimize memory and CPU utilization due to compressed row storage sparse matrix format [83] used for the representation of the Hamiltonian. We also use the package for exact diagonalization developed by Westerhout [84]. In order to construct the TOS for the 19-site supercell, we calculate 512 eigenstates using 2048 Arnoldi vectors for a magnetic field $B = 0.44$. For the classical TOS shown in Fig. 10(c), we also calculate 16 low-lying eigenstates including the ground state using 64 Arnoldi vectors for a magnetic field in the interval [0, 1] with steps $\Delta B = 0.02$. In the case of antiferromagnets, we solve the eigenproblem for each sector of the Hamiltonian separately. For each spin sector of the triangular supercell we perform a full diagonalization, whereas for the square-lattice supercell we calculate 512 low-lying eigenvectors.

[1] D. Home, *Conceptual Foundations of Quantum Physics* (Plenum, New York, 1997).
[2] L. E. Ballentine, *Quantum Mechanics: A Modern Development* (World Scientific, Singapore, 2003).
[3] S. Weinberg, *Lectures on Quantum Mechanics* (Cambridge University Press, Cambridge, England, 2003).
[4] J. S. Bell, *Speakable and Unspeakable in Quantum Mechanics*, 2 ed., (Cambridge University Press, Cambridge, England, 2004).
[5] A. Y. Khrennikov, *Contextual Approach to Quantum Formalism* (Springer, Berlin, 2009).
[6] H. Rauch and S. A. Werner, *Neutron Interferometry: Lessons in Experimental Quantum Mechanics, Wave-Particle Duality, and Entanglement* (Oxford University Press, Oxford, 2015).
[7] K. Landsman, *Foundations of Quantum Theory: From Classical Concepts to Operator Algebras* (Springer, Berlin, 2017).
[8] R. P. Feynman and A. R. Hibbs, *Quantum Mechanics and Path Integrals* (McGraw-Hill, New York, 1965).
[9] H. Kleinert, *Path Integrals in Quantum Mechanics, Statistics, Polymer Physics, and Financial Markets* (World Scientific, Singapore, 2009).
[10] L. S. Schulman, *Techniques and Applications of Path Integration* (Wiley, New York, 1981).
[11] M. Born and E. Wolf, *Principles of Optics*, ed. 7 expanded (Cambridge University Press, Cambridge, England, 1999).
[12] E. Joos and H. D. Zeh, *The emergence of classical properties through interaction with the environment*, Z. Phys. B **59**, 223 (1985).
[13] E. Joos, H. D. Zeh, C. Kiefer, D. J. W. Giulini, J. Kupsch, and I. O. Stamatescu, *Decoherence and the Appearance of a Classical World in Quantum Theory* (Springer, Berlin, 2013).
[14] W. H. Zurek, *Pointer basis of quantum apparatus: Into what mixture does the wave packet collapse?*, Phys. Rev. D **24**, 1516 (1981).
[15] W. H. Zurek, *Decoherence and the transition from quantum to classical*, Phys. Today **44**, No. 10, 36 (1991).
[16] W. H. Zurek, *Decoherence, einselection, and the quantum origins of the classical*, Rev. Mod. Phys. **75**, 715 (2003).

[17] W. H. Zurek, *Quantum Darwinism*, Nat. Phys. **5**, 181 (2009).

[18] *Quantum Theory and Measurement*, edited by J. A. Wheeler and W. H. Zurek (Princeton University Press, Princeton, NJ, 1983).

[19] N. Bohr, *The quantum postulate and recent development of atomic theory*, Nature (London) **121**, 580 (1928).

[20] J. von Neumann, *Mathematical Foundations of Quantum Mechanics* (Princeton University Press, Princeton, NJ, 1955).

[21] M. B. Mensky, *Continuous Quantum Measurements and Path Integrals* (Institute of Physics, Bristol, 1993).

[22] M. I. Katsnelson, V. V. Dobrovitski, and B. N. Harmon, *Propagation of local decohering action in distributed quantum systems*, Phys. Rev. A **62**, 022118 (2000).

[23] S. D. Hamieh and M. I. Katsnelson, *Quantum entanglement dynamics and decoherence wave in spin chains at finite temperatures*, Phys. Rev. A **72**, 032316 (2005).

[24] H. C. Donker, H. De Raedt, and M. I. Katsnelson, *Decoherence wave in magnetic systems and creation of Néel antiferromagnetic state by measurement*, Phys. Rev. B **93**, 184426 (2016).

[25] A. E. Allahverdyan, R. Balian, and T. M. Nieuwenhuizen, *Understanding quantum measurement from the solution of dynamical models*, Phys. Rep. **525**, 1 (2013).

[26] H. C. Donker, H. De Raedt, and M. I. Katsnelson, *Quantum dynamics of a small symmetry breaking measurement device*, Ann. Phys. (Amsterdam) **396**, 137 (2018).

[27] S. V. Vonsovsky, *Magnetism* (Wiley, New York, 1974).

[28] V. Yu. Irkhin and M. I. Katsnelson, *On the description of the antiferromagnetism without anomalous averages*, Z. Phys. B **62**, 201 (1986).

[29] P. W. Anderson, *An approximate quantum theory of the antiferromagnetic ground state*, Phys. Rev. **86**, 694 (1952).

[30] G. Misguich and P. Sindzingre, *Detecting spontaneous symmetry breaking in finite-size spectra of frustrated quantum antiferromagnets*, J. Phys. Condens. Matter **19**, 145202 (2007).

[31] K. Penc, M. Mambrini, P. Fazekas, and F. Mila, *Quantum phase transition in the SU(4) spin-orbital model on the triangular lattice*, Phys. Rev. B **68**, 012408 (2003).

[32] B. Bernu, C. Lhuillier, and L. Pierre, *Signature of Néel order in exact spectra of quantum antiferromagnets on finite lattices*, Phys. Rev. Lett. **69**, 2590 (1992).

[33] A. N. Bogdanov and D. A. Yablonskii, *Thermodynamically stable 'vortices' in magnetically ordered crystals, The mixed state of magnets*, Zh. Eksp. Teor. Fiz. **95**, 178 (1989) [Sov. Phys. JETP **68**, 101 (1989)], http://www.jetp.ras.ru/cgi-bin/dn/e_068_01_0101.pdf.

[34] C. H. Back *et al.*, *The 2020 skyrmionics roadmap*, J. Phys. D **53**, 363001 (2020).

[35] V. V. Mazurenko, Y. O. Kvashnin, A. I. Lichtenstein, and M. I. Katsnelson, *A DMI guide to magnets micro-world*, J. Exp. Theor. Phys. **132**, 506 (2021).

[36] E. A. Stepanov, C. Dutreix, and M. I. Katsnelson, *Dynamical and reversible control of topological spin textures*, Phys. Rev. Lett. **118**, 157201 (2017).

[37] E. A. Stepanov, S. A. Nikolaev, C. Dutreix, M. I. Katsnelson, and V. V. Mazurenko, *Heisenberg-exchange-free nanoskyrmion mosaic*, J. Phys. Condens. Matter **31**, 17LT01 (2019).

[38] K. Wang, Y. Zhang, V. Bheemarasetty, S. Zhou, S.-C. Ying, and G. Xiao, *Single skyrmion true random number generator using local dynamics and interaction between skyrmions*, Nat. Commun. **13**, 722 (2022).

[39] P. Siegl, E. Y. Vedmedenko, M. Stier, M. Thorwart, and T. Posske, *Controlled creation of quantum skyrmions*, Phys. Rev. Res. **4**, 023111 (2022).

[40] A. Derras-Chouk, E. M. Chudnovsky, and D. A. Garanin, *Quantum states of a skyrmion in a two-dimensional antiferromagnet*, Phys. Rev. B **103**, 224423 (2021).

[41] K. Mæland and A. Sudbø, *Quantum fluctuations in the order parameter of quantum skyrmion crystals*, Phys. Rev. B **105**, 224416 (2022).

[42] A. Haller, S. Groenendijk, A. Habibi, A. Michels, and T. L. Schmidt, *Quantum skyrmion lattices in Heisenberg ferromagnets*, Phys. Rev. Res. **4**, 043113 (2022).

[43] J. P. Gauyacq and N. Lorente, *A model for individual quantal nano-skyrmions*, J. Phys. Condens. Matter **31**, 335001 (2019).

[44] V. Lohani, C. Hickey, J. Masell, and A. Rosch, *Quantum skyrmions in frustrated ferromagnets*, Phys. Rev. X **9**, 041063 (2019).

[45] O. M. Sotnikov, V. V. Mazurenko, J. Colbois, F. Mila, M. I. Katsnelson, and E. A. Stepanov, *Probing the topology of the quantum analog of a classical skyrmion*, Phys. Rev. B **103**, L060404 (2021).

[46] R. A. Istomin and A. S. Moskvin, *Overlap integral for quantum skyrmions*, Pis'ma Zh. Eksp. Teor. Fiz. **71**, 487 (2000).

[47] A. M. Perelomov, *Generalized Coherent States and Their Applications* (Springer-Verlag, Berlin, 1986).

[48] A. Inomata, H. Kuratsuji, and C. C. Cherry, *Path Integrals and Coherent States of SU(2) and SU(1,1)* (World Scientific, Singapore, 1990).

[49] S. Heinze, K. von Bergmann, M. Menzel, J. Brede, A. Kubetzka, R. Wiesendanger, G. Bihlmayer, and S. Blügel, *Spontaneous atomic-scale magnetic skyrmion lattice in two dimensions*, Nat. Phys. **7**, 713 (2011).

[50] M. A. Nielsen and I. L. Chuang, *Quantum Computation and Quantum Information* (Cambridge University Press, Cambridge, England, 2010).

[51] A. Wietek, M. Schuler, and A. M. Läuchli, *Studying continuous symmetry breaking using energy level spectroscopy*, arXiv:1704.08622.

[52] L. de Forges de Parny, H. Yang, and F. Mila, *Anderson tower of states and nematic order of spin-1 bosonic atoms on a 2D lattice*, Phys. Rev. Lett. **113**, 200402 (2014).

[53] J. Villain, *A magnetic analogue of stereoisomerism: Application to helimagnetism in two dimensions*, J. Phys. (Paris) **38**, 385 (1977).

[54] P. W. Leung and K. J. Runge, *Spin-$\frac{1}{2}$-quantum antiferromagnets on the triangular lattice*, Phys. Rev. B **47**, 5861 (1993).

[55] G. Carleo and M. Troyer, *Solving the quantum many-body problem with artificial neural networks*, Science **355**, 602 (2017).

[56] T. Westerhout, N. Astrakhantsev, K. S. Tikhonov, M. I. Katsnelson, and A. A. Bagrov, *Generalization properties of neural network approximations to frustrated magnet ground states*, Nat. Commun. **11**, 1593 (2020).

[57] H. Nishimori and H. Nakanishi, *Ground state of quantum spin systems on the triangular lattice*, J. Phys. Soc. Jpn. **57**, 626 (1988).
[58] P. Azaria, B. Delamotte, and D. Mouhanna, *Spontaneous symmetry breaking in quantum frustrated antiferromagnets*, Phys. Rev. Lett. **70**, 2483 (1993).
[59] R. Wiesendanger, *Spin mapping at the nanoscale and atomic scale*, Rev. Mod. Phys. **81**, 1495 (2009).
[60] X. Z. Yu, Y. Onose, N. Kanazawa, J. H. Park, J. H. Han, Y. Matsui, N. Nagaosa, and Y. Tokura, *Real-space observation of a two-dimensional skyrmion crystal*, Nature (London) **465**, 901 (2010).
[61] H. Everett III, *'Relative state' formulation of quantum mechanics*, Rev. Mod. Phys. **29**, 454 (1957).
[62] J. A. Wheeler, *Assessment of Everett's 'relative state' formulation of quantum theory*, Rev. Mod. Phys. **29**, 463 (1957).
[63] H. Hafermann, M. I. Katsnelson, and A. I. Lichtenstein, *Metal-insulator transition by suppression of spin fluctuations*, Europhys. Lett. **85**, 37006 (2009).
[64] H. C. Donker, H. De Raedt, and M. I. Katsnelson, *Antiferromagnetic order without recourse to staggered fields*, Phys. Rev. B **98**, 014416 (2018).
[65] P. Lecheminant, B. Bernu, C. Lhuillier, and L. Pierre, $J_1 - J_2$ *quantum Heisenberg antiferromagnet on the triangular lattice: A group-symmetry analysis of order by disorder*, Phys. Rev. B **52**, 6647 (1995).
[66] V. Vanchurin, Y. I. Wolf, M. I. Katsnelson, and E. V. Koonin, *Toward a theory of evolution as multilevel learning*, Proc. Natl. Acad. Sci. U.S.A. **119**, e2120037119 (2022).
[67] V. Vanchurin, Y. I. Wolf, E. V. Koonin, and M. I. Katsnelson, *Thermodynamics of evolution and the origin of life*, Proc. Natl. Acad. Sci. U.S.A. **119**, e2120042119 (2022).
[68] L.-M. Duan, E. Demler, and M. D. Lukin, *Controlling spin exchange interactions of ultracold atoms in optical lattices*, Phys. Rev. Lett. **91**, 090402 (2003).
[69] S. Trotzky, P. Cheinet, S. Fölling, M. Feld, U. Schnorrberger, A. M. Rey, A. Polkovnikov, E. A. Demler, M. D. Lukin, and I. Bloch, *Time-resolved observation and control of superexchange interactions with ultracold atoms in optical lattices*, Science **319**, 295 (2008).
[70] X.-s. Ma, B. Dakić, S. Kropatschek, W. Naylor, Y.-h. Chan, Z.-x. Gong, L.-m. Duan, A. Zeilinger, and P. Walther, *Towards photonic quantum simulation of ground states of frustrated Heisenberg spin systems*, Sci. Rep. **4**, 3583 (2014).
[71] K. Kim, M.-S. Chang, S. Korenblit, R. Islam, E. E. Edwards, J. K. Freericks, G.-D. Lin, L.-M. Duan, and C. Monroe, *Quantum simulation of frustrated Ising spins with trapped ions*, Nature (London) **465**, 590 (2010).
[72] J. Struck, C. Ölschläger, R. Le Targat, P. Soltan-Panahi, A. Eckardt, M. Lewenstein, P. Windpassinger, and K. Sengstock, *Quantum simulation of frustrated magnetism in triangular optical lattices*, Science **333**, 996 (2011).
[73] A. A. Khajetoorians, J. Wiebe, B. Chilian, and R. Wiesendanger, *Realizing all-spin-based logic operations atom by atom*, Science **332**, 1062 (2011).
[74] L. K. Grover, in *Proceedings of the 28th Annual ACM Symposium on the Theory of Computing, Philadelphia, 1996*, (Association for Computing Machinery, New York, 1996), p. 212.
[75] *Code examples for triangular lattice antiferromagnet*, 10.5281/zenodo.7265441.
[76] Fengshan Zheng, Nikolai S. Kiselev, Luyan Yang, Vladyslav M. Kuchkin, Filipp N. Rybakov, Stefan Blügel, and Rafal E. Dunin-Borkowski, *Skyrmion-antiskyrmion pair creation and annihilation in a cubic chiral magnet*, Nat. Phys. **18**, 863 (2022).
[77] I. A. Iakovlev, O. M. Sotnikov, and V. V. Mazurenko, *Supervised learning approach for recognizing magnetic skyrmion phases*, Phys. Rev. B **98**, 174411 (2018).
[78] I. A. Iakovlev, O. M. Sotnikov, and V. V. Mazurenko, *Profile approach for recognition of three-dimensional magnetic structures*, Phys. Rev. B **99**, 024430 (2019).
[79] A. A. Bagrov, I. A. Iakovlev, A. A. Iliasov, M. I. Katsnelson, and V. V. Mazurenko, *Multiscale structural complexity of natural patterns*, Proc. Natl. Acad. Sci. U.S.A. **117**, 30241 (2020).
[80] O. M. Sotnikov, I. A. Iakovlev, A. A. Iliasov, M. I. Katsnelson, A. A. Bagrov, and V. V. Mazurenko, *Certification of quantum states with hidden structure of their bitstrings*, npj Quantum Inf. **8**, 41 (2022).
[81] A. Wietek and A. M. Läuchli, *Sublattice coding algorithm and distributed memory parallelization for large-scale exact diagonalizations of quantum many-body systems*, Phys. Rev. E **98**, 033309 (2018).
[82] G. Ian, P.-A. Jean, M. Mehdi, X. Bing, W.-F. David, O. Sherjil, C. Aaron, and B. Yoshua, *Generative adversarial nets*, in *Proceedings of the International Conference on Neural Information Processing Systems (NIPS 2014)* (Curran Associates, Inc., New York, 2014), pp. 2672–2680.
[83] J. D. Z. Bai, J. Dongarra, A. Ruhe, and H. van der Vorst, *Templates for the Solution of Algebraic Eigenvalue Problems: A Practical Guide* (Society for Industrial and Applied Mathematics, Philadelphia, 2000).
[84] T. Westerhout, *Lattice-symmetries: A package for working with quantum many-body bases*, J. Open Source Softwaare **6**, 3537 (2021).